Spectral and spatial evolution of a conical emission in Na vapor

A. Dreischuh,* V. Kamenov,* S. Dinev,* U. Reiter-Domiaty, D. Gruber, and L. Windholz

Institut für Experimentalphysik, Technische Universität Graz, Petersgasse 16, 8010 Graz, Austria

Received July 1, 1997

A detailed study on yellow conical emission observed in dense sodium vapor following near-resonant one-photon excitation of the Na 4^2P levels was performed. The origins of conical emission are suggested to be due to Raman resonant four-wave parametric mixing processes. In order to describe spectral and spatial features of off-axis emission, we introduce self-phase modulation and induced-phase modulation as important additional nonlinear processes, explaining the nonmonotonic detuning of the wavelength of the conical radiation with the exiting laser wavelength in the vicinity of resonance transitions. The spatial evolution of emission generated via four-wave mixing is modeled by solving the two-dimensional nonlinear Schrödinger equation describing the spatial evolution of light beams in a nonlinear media. Experimental and theoretical results are presented and discussed. © 1998 Optical Society of America [S0740-3224(98)01901-8]

OCIS codes: 190.4410, 190.5940, 300.2570, 300.6210.

1. INTRODUCTION

Conical emission, arising from alkali metal vapor following near-resonant pulsed laser excitation, associated with spectral line broadening, frequency shift of emission, and cone angle variation with respect to the wavelength of the exciting laser pulse and self-action processes in the nonlinear medium, has been the subject of numerous experimental and theoretical considerations over the past two decades. Various effects, mainly based on radiation generation via parametric wave mixing, three-photon scattering and temporal pulse reshaping of Rabi-sideband amplification,[1–6] stimulated Raman[7] and hyperfine Raman scattering accompanied by self-phase modulation,[8] pulse breakup into solitary waves,[9] Cerenkov-like radiation generation[10–13] and diffraction-free encoding followed by free space propagation[14] have been taken into account to describe conical emission features and origins of off-axis emission-generation processes. Valley *et al.*[15] achieved the first good agreement between experimental data and theoretical calculations assuming four-wave parametric mixing (FWPM) and diffraction spreading initiated by resonance fluorescence of uncorrelated atoms during propagation of the light through the nonlinear medium.

In this work we present a qualitative description of the nonmonotonic spectral tuning of the conical radiation for the exciting laser tuned across the 3^2S-4^2P resonances. Based on the FWPM model for the origin of conical emission,[6] spectral characteristics of off-axis radiation are discussed with respect to nonlinear resonant-enhanced self-phase modulation (SPM) and induced-phase modulation (IPM) of waves involved in the radiation-generation process.

Further, we modeled spatial features of conical emission in the FWPM process as a consequence of the spatiotemporal dynamics described by the nonlinear Schrödinger equation[16] (NLSE) owing to dispersion and sign change of the third-order susceptibility for SPM in the parametric wave-mixing process. Standard analytical techniques failed to resolve the strongly coupled space and time dynamics captured by the Schrödinger equation; therefore a two-dimensional (2D) generalization of the split-step Fourier method is used for numerical studies.

The self-consistent treatment of all the waves involved requires a coherently coupled system of four $(2+1)$D NLSEs to be solved by 16 fast-Fourier transformations per each computational step along the nonlinear medium. In addition to high memory and CPU-speed requirements, our attempts to account correctly for the dispersion of the nonlinear coefficients for SPM and IPM have led to an unacceptable reduction of the accuracy of the numerical procedure. Therefore we later restricted our calculations to the simpler method mentioned above. Since these simple simulations are in good agreement with experimental observations, we emphasize that SPM and IPM are of fundamental importance for the properties of conical emission.

2. EXPERIMENTAL SETUP

The experimental setup used is similar to that described in Ref. 17. Briefly, sodium is heated up to 300–550 °C (corresponding to vapor densities N of approximately 10^{15} cm^{-3}–10^{17} cm^{-3}, respectively) in a heat-pipe oven within a sodium-vapor column interaction region of ~6 cm. Argon is added as buffer gas with typical pressures of 50–55 mbars. Sodium vapor is excited by focused dye-laser pulses in the wavelength range between 328.8 and 331.6 nm. Emission spectra of conical radiation are recorded by a 50-cm monochromator/spectrograph equipped with a 1200-grooves/mm grating and a 1024-diode array optical multichannel analyzer. Central or off-axially emitted light is selected for analysis by the use of appropriate diaphragms placed right after the output window of the heat-pipe oven. The spatial distribution of the conical emission is recorded with a CCD color video camera, located 98 cm in front of a trans-

0740-3224/98/010034-07$10.00

parent screen, placed 43 cm behind the output window of the heat pipe. Subsequently data are transferred to a personal computer via a frame grabber.

3. RESULTS

Figure 1 shows the Na levels involved in the emission-generation processes upon near-resonant excitation. Taking into account that no temporal delay could be resolved between conical emission and exciting laser-pulse radiation within 2 ns (resolution of the detection system) and that the time behavior of conical radiation closely reproduces that of the laser pulse, nonlinear processes are emphasized to be responsible for the generation of the observed emission. Conical emission is obtained from both, $3S-4P-4S-3P$ and $3S-4P-3D-3P$ transition cascades. Besides conical radiation ascribed to this FWPM process enhanced by stimulated electronic Raman scattering via Na $4P_{1/2,3/2}$ intermediate levels, a second off-axis radiation can be observed owing to four-wave parametric amplification of the Rabi sidebands of the $3S-3P$ transition.[16,17] In this work we concentrate on describing the dependence of cone angle and conical radiation wavelength upon laser detuning, according to phase-matching considerations within the FWPM process.[18] The experimental data are discussed, and model studies are performed.

A. Spectral Behavior of the Conical Emission

Figure 2 presents emission spectra of conical radiation recorded in the vicinity of the Na D lines for the laser light tuned from 329.05 to 330.5 nm. The characteristic features of these spectra of the conical emission observed can be summarized in three main topics:

(i) Broadband conical radiation on the red side of the D_1 line is observed for both blue and red detuning of the pump laser from the $3^2S_{1/2}-4^1P_{1/2}$ (λ=330.298 nm) and $3^2S_{1/2}-4^1P_{3/2}$ (λ=330.223 nm) resonances [Figs. 2(a) and 2(b)].

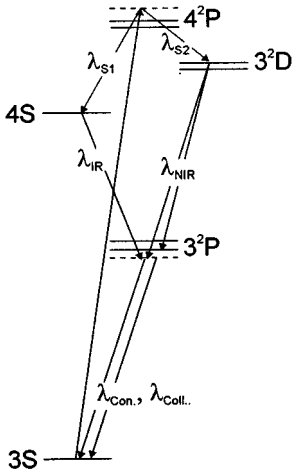

Fig. 1. Simplified Na energy-level diagram with a scheme of the FWPM processes observed.

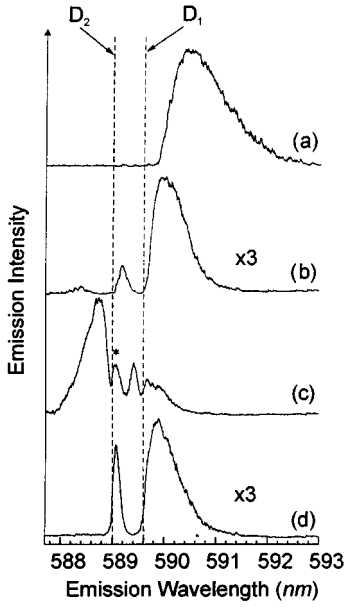

Fig. 2. Typical spectra of the yellow emission around the Na D lines for different values of the exciting laser wavelength λ_L (a) 329.05-nm, (b) 330.50-nm, (c) 329.90-nm, and (d) 330.10-nm.

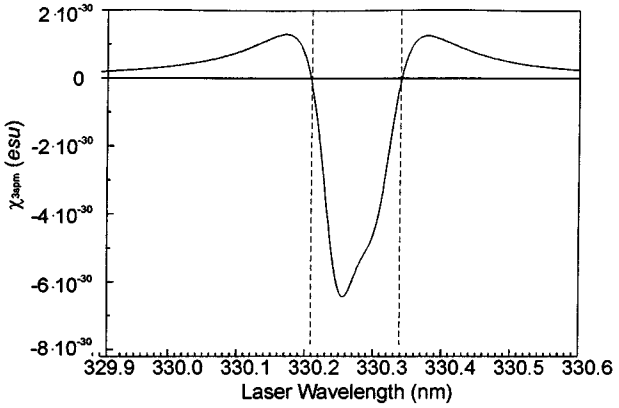

Fig. 3. Third-order nonlinear susceptibility for laser SPM versus wavelength (horizontal solid and vertical dashed lines indicate the wavelengths, at which the susceptibility changes its sign).

(ii) When tuning the laser frequency closer to the resonance lines, the emission wavelength tunes first closer to the D_1 line [Fig. 2(c)] and later on again away from it [Fig. 2(d)].

(iii) For the laser frequency tuned between the Na $3S-4P$ transition, the first mentioned broadband emission nearly vanishes, but another conical emission is observed only on the blue side of the D_2 line [Fig. 2(c)].

Conical radiation approaches the Na D_2 resonance line while decreasing the blue detuning of the laser from Na $3S-4^2P_{3/2}$ transition (330.237 nm) and tunes away from the Na D_2 transition when increasing the red detuning of the laser from $3S-4^2P_{1/2}$ resonance (330.298 nm). Conical radiation owing to this FWPM process is observed for laser wavelengths ranging from 328.8 to 331.6 nm. At λ_L = 330.10 nm a second spectrally offset emission, assumed to be created by an induced FWPM process within

the first Na resonance transitions, is recorded and denoted with a star in Fig. 2 but is not discussed within the frame of this work. Collimated emissions observed on atomic transitions are identified as amplified spontaneous-emission cascades.[6]

All features of the conical emission observed give strong evidence on the existence of a linear intensity-dependent angular phase matching, corresponding to a vector synchronism of the type

$$\mathbf{k}_{\mathrm{L}} = \mathbf{k}_{\mathrm{IR}} + \mathbf{k}_{\mathrm{R}} + \mathbf{k}_{\mathrm{Y}}. \tag{1}$$

In order to simplify the notation, we denote the $3S-4P$ transition as laser (L), the Stokes radiation ($4P-4S$ and $4P-3D$) as infrared (IR) emission, the $4S-3P$ ($3D-3P$) as red (R), and the $3P-3S$ transition as yellow (Y) emission, respectively.

Because radiation owing to k_Y is observed on a conical shell with respect to the laser propagation axis, the wave-vector synchronism of Eq. (1) requires at least a second wave with an angular offset. Assuming that the Stokes radiation involved in the Raman-resonant FWPM process is mainly amplified along the laser pulse propagation axis in the heat pipe, red emissions ($4S-3P$, $3D-3P$) are considered to form conical ring patterns when propagating through the nonlinear medium. The particular value of the scalar wave-vector mismatch $\Delta\mathbf{k}^{\mathrm{L}}$, depending on the beam-focusing conditions ($\Delta\mathbf{k}^{\mathrm{L}} = 0$ at incident plane waves),[19] can be extracted from conical-emission geometry at low pump-laser pulse intensities.

Besides the FWPM process investigated, an observed asymmetrical spectral feature of the laser pulse after propagation through the sodium vapor indicates the presence of accompanying nonlinear processes. Therefore SPM and IPM are taken into account as additional nonlinear, resonant-enhanced processes accompanying FWPM emission generation.[20]

To investigate the influence of SPM and IPM on the features of conical emission, we consider an optical wave of intensity I propagating through the optical medium. The self-action of the incident beam, caused by the change of the medium refractive index $n = n_0 + n_2 I$ (n_2 designed as the nonlinear refractive-index coefficient), is responsible for the SPM effect observed. In the presence of two intense waves the refractive index at the ith wavelength is described by

$$n(\lambda_i) = n_0(\lambda_i) + n_2^{\mathrm{SPM}}(\lambda_i) I_i + n_2^{\mathrm{IPM}}(\lambda_i) I_j, \quad i, j = 1, 2;\ i \neq j. \tag{2}$$

Therefore refractive-index variation can be induced between the copropagating waves (IPM). Taking into account that third-order nonlinear susceptibilities $\chi^{(3)}$ ($\propto n_2$) have extremely high values in the vicinity of resonances,[21] these processes can significantly modify the linear scalar wave-vector mismatch $\Delta\mathbf{k}^{\mathrm{L}}$.[22]

The influence of the scalar nonlinear correction $\Delta\mathbf{k}^{\mathrm{NL}}$ to the mismatch $\Delta\mathbf{k} = \Delta\mathbf{k}^{\mathrm{L}} + \Delta\mathbf{k}^{\mathrm{NL}}$ is explained by following considerations:

Taking into account only Na $3S-4P-4S-3P$ and $3S-4P-3D-3P$ cascades, the corresponding nonlinear parts of the laser, infrared, red, and yellow emission wave vectors are given by

$$k_{\mathrm{N}}^{\mathrm{NL}} = k_{\mathrm{L}}\{n_{\mathrm{SPM}}^{\mathrm{L}} I_{\mathrm{L}} + n_{\mathrm{IPM}}^{\mathrm{L,IR}} I_{\mathrm{IR}} + n_{\mathrm{IPM}}^{\mathrm{L,Y}} I_{\mathrm{Y}}\}, \tag{3a}$$

$$k_{\mathrm{IR}}^{\mathrm{NL}} = k_{\mathrm{IR}}\{n_{\mathrm{SPM}}^{\mathrm{IR}} I_{\mathrm{IR}} + n_{\mathrm{IPM}}^{\mathrm{IR,L}} I_{\mathrm{L}} + n_{\mathrm{IPM}}^{\mathrm{IR,R}} I_{\mathrm{R}}\}, \tag{3b}$$

$$k_{\mathrm{R}}^{\mathrm{NL}} = k_{\mathrm{L}}\{n_{\mathrm{SPM}}^{\mathrm{R}} I_{\mathrm{R}} + n_{\mathrm{IPM}}^{\mathrm{R,IR}} I_{\mathrm{IR}} + n_{\mathrm{IPM}}^{\mathrm{R,Y}} I_{\mathrm{Y}}\}, \tag{3c}$$

$$k_{\mathrm{Y}}^{\mathrm{NL}} = k_{\mathrm{L}}\{n_{\mathrm{SPM}}^{\mathrm{Y}} I_{\mathrm{Y}} + n_{\mathrm{IPM}}^{\mathrm{Y,R}} I_{\mathrm{R}} + n_{\mathrm{IPM}}^{\mathrm{Y,L}} I_{\mathrm{L}}\}, \tag{3d}$$

where $n_{\mathrm{SPM}}^{j,k}$ and $n_{\mathrm{IPM}}^{j,k}$ denote the nonlinear coefficients for SPM/IPM of the jth wave originating from the kth wave. In this notation the scalar nonlinear correction to the wave-vector mismatch can be written as

$$\Delta\mathbf{k}^{\mathrm{NL}} = k_{\mathrm{L}}^{\mathrm{NL}} - (k_{\mathrm{IR}}^{\mathrm{NL}} + k_{\mathrm{R}}^{\mathrm{NL}} + k_{\mathrm{Y}}^{\mathrm{NL}}). \tag{4}$$

In order to provide a satisfactory description of the spectral features of the conical radiation, we have to explain the fact that the off-axis radiation is observed for the exciting laser wavelengths not only tuned to the blue[14] but also to the red side of $3S-4^2P$ resonance transitions. Therefore we demonstrate that the tuning of the conical emission always ensures the lowest values of $|\Delta\mathbf{k}^{\mathrm{NL}}|$, i.e., the weakest modification of the linear intensity-dependent phase matching in the FWPM process even in case of near-resonant excitation of the medium.

The population of the $3D$, $4S$, and $3P$ levels owing to the parametric process described above should be low. Nonlinear processes of SPM and IPM starting from these levels should be negligible (e.g., the IPM of the infrared wave by the red one described by the term $n_{\mathrm{IPM}}^{\mathrm{IR,R}} = n_{\mathrm{IPM}}^{\mathrm{R,IR}}$). SPM and IPM between infrared and red emissions starting from the ground level correspond to $2\omega_{\mathrm{IR}}$, $2\omega_{\mathrm{R}}$, and $\omega_{\mathrm{R}}+\omega_{\mathrm{IR}}$, located far from any two-photon resonances. Since the intensity of the yellow emission is much smaller than the laser intensity I_{L}, the term $n_{\mathrm{IPM}}^{\mathrm{L,Y}} I_{\mathrm{Y}}$ in Eq. (3) can be neglected compared with the term $n_{\mathrm{IPM}}^{\mathrm{Y,L}} I_{\mathrm{L}}$. The same considerations hold for the terms comprising the intensities of the infrared emissions. Here a branching into $4P-4S-3P$ and $4P-3D-3P$ takes place.

Taking into account that the laser pulse is the most intense of all waves contributing to processes, Eq. (4) can be simplified to

$$\Delta\mathbf{k}^{\mathrm{NL}} = \{k_{\mathrm{L}} n_{\mathrm{L}}^{\mathrm{SPM}} - k_{\mathrm{IR}} n_{\mathrm{IPM}}^{\mathrm{IR,L}} - k_{\mathrm{Y}} n_{\mathrm{IPM}}^{\mathrm{Y,L}}\} I_{\mathrm{L}}. \tag{5}$$

This result is characterized by an interesting feature: According to these approximations, absorption of the pump laser does not contribute to the balanced counteractions of the nonlinear corrections investigated. Therefore if the condition

$$\Delta\mathbf{k}^{\mathrm{NL}}(\lambda_{\mathrm{L}}, \lambda_{\mathrm{Y}}, \lambda_{\mathrm{IR}}) = 0$$

is satisfied at the beginning of the nonlinear interaction zone (sodium vapor column), it is satisfied along the whole interaction path. Therefore Eq. (5) can be transformed to

$$\lambda_{\mathrm{L}}^{-1} \chi_{\mathrm{SPM}}^{(3)}(\lambda_{\mathrm{L}}) - \lambda_{\mathrm{IR}}^{-1} \chi_{\mathrm{IPM}}^{(3)}(\lambda_{\mathrm{IR}}\lambda_{\mathrm{L}}) - \lambda_{\mathrm{Y}}^{-1} \chi_{\mathrm{IPM}}^{(3)}(\lambda_{\mathrm{Y}}\lambda_{\mathrm{L}}) = 0, \tag{6}$$

where $\chi^{(3)}_{SPM}(\lambda_j;\lambda_L)$ and $\chi^{(3)}_{IPM}(\lambda_j;\lambda_L)$ denote the third-order nonlinear susceptibilities for SPM of the laser and for IPM of the jth wave (infrared, yellow) by the laser pulse.

In order to define the wavelength range, for which Eq. (6) is satisfied, we calculate the dispersion curves of the nonlinear susceptibility $\chi^{(3)}_{SPM}(\lambda_L)$ related to pump-laser SPM as well as dispersion curves of $\chi^{(3)}_{IPM}$ of the infrared (Fig. 4) and the yellow (Fig. 5) emissions [$\chi^{(3)}_{IPM}(\lambda_{IR};\lambda_L)$ and $\chi^{(3)}_{IPM}(\lambda_Y;\lambda_L)$]. The calculation is based on a set of Feynman diagrams for the process investigated.[23] Sixteen allowed transitions between levels playing the major role in the SPM/IPM processes are taken into account. The damping constants of the transitions were extracted from the experimental data. The accuracy of our calculation of the third-order susceptibilities is estimated to 40%. Results, presented in Fig. 4, show that $\chi^{(3)}_{SPM}(\lambda_L)$ and $\chi^{(3)}_{IPM}(\lambda_{IR};\lambda_L)$ change their signs nearly at the same detuning from $3S-3P$ resonances but are distinguished by opposite signs. This behavior of the nonlinear susceptibilities indicates that the first two terms in Eq. (6) should also be influenced by the dispersion of $\chi^{(3)}_{IPM}(\lambda_Y;\lambda_L)$ (Fig. 5).

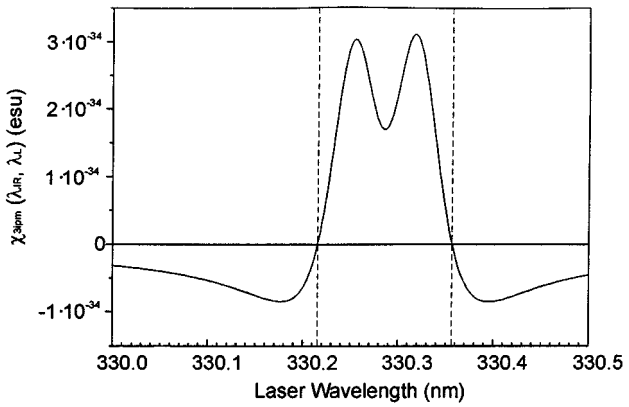

Fig. 4. Third-order nonlinear susceptibility for IPM of the infrared emission (wavelength $\lambda_{IR} = 9140.96\,nm$) versus laser wavelength (the solid and dashed lines have the same meaning as those in Fig. 3).

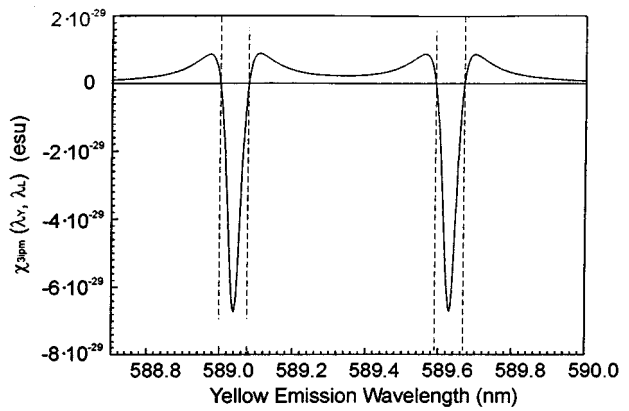

Fig. 5. Dispersion of the third-order nonlinear susceptibility for IPM of the yellow emission at a specific laser wavelength $\lambda_L = 330.298$ nm. (The solid and dashed lines have the same meaning as those in Fig. 3).

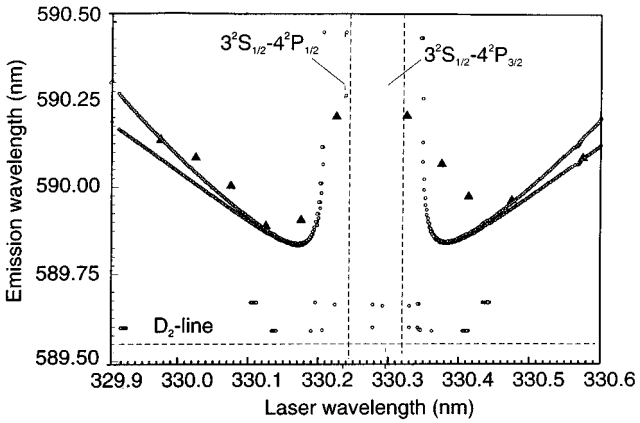

Fig. 6. Center-of-gravity wavelength of the conical emission versus the pump-laser wavelength retrieved from the experimental data. Circles indicate numerically obtained solutions of Eq. (5), based on the $\chi^{(3)}_{SPM}$ dispersion curves shown in Figs. 3–5.

According to reductions made throughout analysis and with respect to the uncertainty of the nonlinear susceptibilities, we required Eq. (6) to be satisfied within an accuracy of 10^{-34} esu simultaneously for both the $3S-4P-4S-3P$ and $3S-4P-3D-3P$ cascades. Results of this calculation (circles) and experimental data (up triangles) are plotted in Fig. 6.

For laser wavelengths tuned toward $3^2S_{1/2}-4^2P_{1/2}$ resonance, the center-of-gravity wavelength of the conical emission approaches the sodium D_2 line, but very close to resonant excitation, emission again detunes from the D_2 value toward higher wavelengths. Qualitatively, the same behavior of the yellow conical emission is found for the pump wavelengths tuned to the $3^2S_{1/2}-4^2P_{3/2}$ line from higher wavelengths. These results demonstrate that the wavelength of the yellow conical emission follows conditions, under which the nonlinear SPM and IPM accompanying the FWPM does not influence the linear intensity-independent vector synchronism of the parametric mixing. The stability of the curves resulting from calculation was proved by increasing the accuracy required up to 2 orders of magnitude.

B. Spatial Evolution

As expected for a FWPM process, the cone-angle of emission is proportional to $1/\sqrt{\Delta\lambda}$ as long as laser wavelength detuning from resonance is larger than $\Delta\lambda = 0.1$ nm. Experimental observations show a decreasing cone angle for detunings $\Delta\lambda < 0.1$ nm. To obtain an understanding of this effect, we treat this behavior of the spatial distribution of the conical emission as the result of a SPM effect and present numerical simulations supporting our interpretations, at least qualitatively. In Fig. 7 the dependence of the cone angle on laser wavelength is shown.

In Subsection 3.A, self-action processes owing to conical emission and their contribution to Δk^{NL} were neglected, since the laser pulse was the most intense wave in the process investigated. Nevertheless, in the vicinity of the D_2 resonance line the nonlinear susceptibility for SPM significantly changes its absolute value $|\chi^{(3)}_{SPM}(\lambda_L)|$ and sign. The importance of taking SPM into account for detunings in the vicinity of resonance has to be emphasized because of the following:

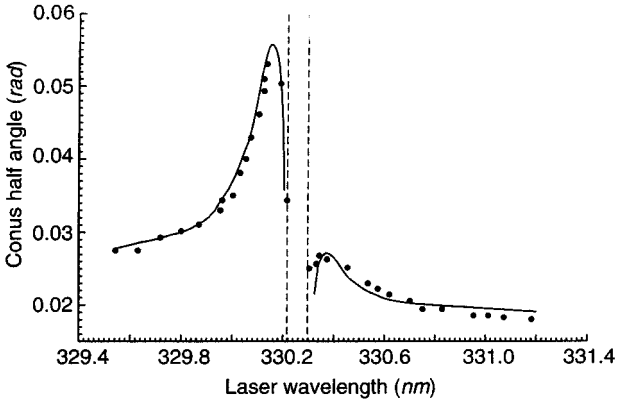

Fig. 7. Conical radiation half-angle in dependence of the laser wavelength (points indicate measured values, and the solid curve indicates calculation).

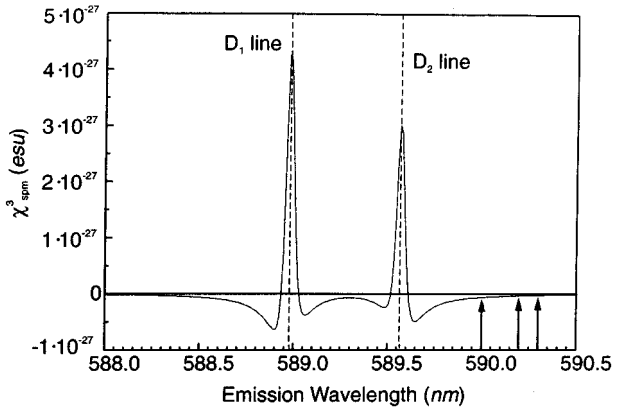

Fig. 8. Dispersion of the third-order nonlinear susceptibility for SPM in the vicinity of the Na first fine-structure doublet. (The solid line indicates the sign-change of $\chi^{(3)}_{\mathrm{SPM}}$ and the dashed line indicates the Na D lines). The arrows denote the wavelengths λ_{Y}, at which the numerical simulations shown in Figs. 9–11 are carried out.

(i) Even in the case of the lowest detuning of the yellow emission from the sodium $4^2P_{3/2}$ resonance transition ($\sim$0.1 nm), the condition for a more dispersive than absorptive nonlinearity (the real part of the nonlinearity is larger than the imaginary part) is still satisfied.[24]

(ii) The real part of the Kerr coefficient $n_2^{\mathrm{SPM}}(\lambda_Y)$ [see Eq. (2)] depends on the inverse of the third power of the detuning from the line center.[24]

In Fig. 8 we demonstrate a numerical estimation of the dispersion of third-order nonlinear susceptibility for SPM near the Na $3^2P_{1/2,3/2}$ transitions. At $\Delta\lambda < 0.4$ nm, resonances enhance $|\chi^{(3)}_{\mathrm{SPM}}|$ in orders of magnitude.

It is natural to expect that the tuning behavior of the conical emission under such a significant dispersion of $\chi^{(3)}_{\mathrm{SPM}}$ can lead to profile changes of the conical beam/pulse in time and space. Since nanosecond pulses are involved, it is difficult to observe significant changes in the shapes of the yellow pulses.[25] However, resonantly enhanced spatial self-action in alkali vapors is known to cause self-defocusing of bright intense beams.[26]

The evolution of the spatial distribution of the yellow conical emission is modeled on the base of the nonlinear Schrödinger equation

$$i\frac{\partial A}{\partial z} + \frac{1}{2L_D}\left(\frac{\partial^2}{\partial x^2} + \frac{\partial^2}{\partial y^2}\right)A + \frac{\mathrm{sign}[n_2^{\mathrm{SPM}}(\lambda_{\mathrm{Y}})]}{L_{\mathrm{NL}}}|A|^2A = 0, \quad (7)$$

where z is the coordinate along the nonlinear propagation path (Na-vapor column), x and y are the transverse coordinates, A is the slowly varying electric-field amplitude, and sign $[n_2^{\mathrm{SPM}}(\lambda_Y)] = -1$. The diffraction length L_{D} and nonlinear length L_{NL} are related to the wave number k_{Y}, conical ring width r_0, and nonlinear correction $|n_2^{\mathrm{SPM}}|I$ to the linear refractive index since

$$L_{\mathrm{D}} = kr_0{}^2, \quad (8a)$$

$$L_{\mathrm{NL}} = (k|n_2^{\mathrm{SPM}}|I)^{-1}. \quad (8b)$$

We solve Eq. (7) by using a (2 + 1)—dimensional generalization of the split-step Fourier method (beam propagation method) over 512 × 512 grid points with the temporal coordinate treated as a parameter. Since pictures recorded by the video camera are time integrated, in our simulation, time integration is expanded over 64 time slices of 2D ring emissions. To obtain a convenient qualitative similarity with the experimental data, we modeled the nonlinear evolution of two bright coaxial rings of the form

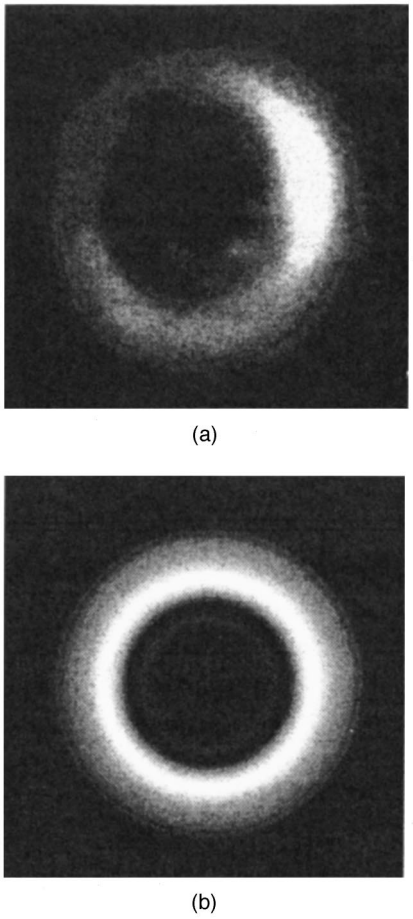

Fig. 9. Gray-scale patterns of the yellow conical emission recorded experimentally (a) at $\lambda_{\mathrm{L}} = 329.65$ nm ($\lambda_{\mathrm{Y}} = 590.3$ nm) and (b) generated numerically.

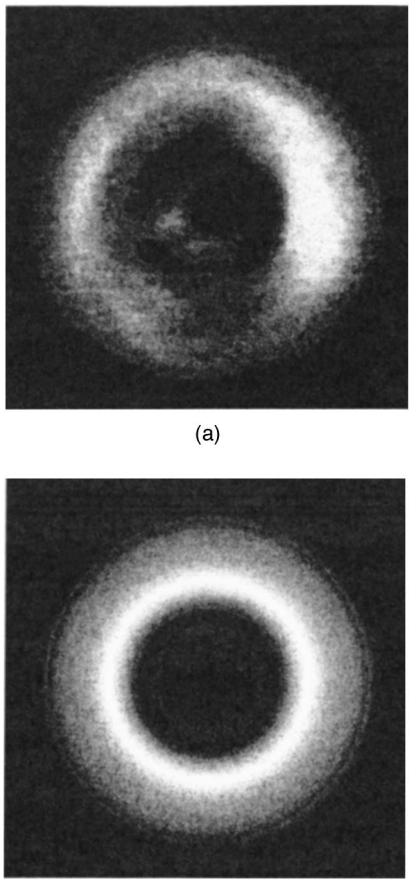

(a)

(b)

Fig. 10. Same as in Fig. 10 for $\lambda_L = 329.53$ nm ($\lambda_Y = 590.2$ nm).

$$A = \left\{ A_1 \exp\left[-\frac{(r - R_1)^2}{r_0^2} \right] + A_2 \exp\left[-\frac{(r - R_2)^2}{r_0^2} \right] \right\} \exp(-t^2) \qquad (9)$$

(with $r^2 = x^2 + y^2$ and t standing for the normalized time), one ring originating in the FWPM process, and the second in the FWP amplification of the Rabi sidebands of the $3S-3P$ transition. The particular parameters of the model are $R_1/R_2 = 1.2$ and $A_1/A_2 = 2$. It was accounted also that, after the 6-cm-long nonlinear propagation path inside the heat-pipe ($z = 0.5L_D$), the regime of propagation does change to a linear one influenced only by the diffraction to the screen ($z = 1.0L_D$). The resonant character of $n_2^{SPM}(\lambda_Y) \approx \chi^{(3)}_{SPM}(\lambda_Y)$ (see Fig. 8) is accounted for by use of the particular pump-laser wavelength λ_L, at which the 2D transverse energy-density distribution is recorded and deduced by the center-of-gravity wavelength of the yellow conical emission λ_Y (see also Fig. 9).

Figure 9 shows a plot of the 2D ring pattern of the conical emission experimentally recorded at (a) $\lambda_L = 329.65$ nm ($\lambda_Y = 590.3$ nm) and (b) numerically generated at $L_{NL}/L_D = 0.5$. The bright ring SPM in a self-defocusing nonlinear medium causes an enhancement of the off-axis radiation width and the decrease of its radius. Based on these results, we modeled the conical ring pattern [Fig. 10(a)] observed at $\lambda_L = 329.53$ nm ($\lambda_Y = 590.2$ nm) by modifying the value of $n_2^{SPM}(\lambda_Y)$ by a factor of 4 (see Fig. 8, arrows). The ring diameter [Fig. 10(b)] is found to decrease further with broadening of the ring arc, but the central part of the pattern remains dark. The experimentally observed spatial distribution of the yellow emission at $\lambda_L = 329.825$ nm ($\lambda_Y = 590.0$ nm) [a simulation result is demonstrated in Fig. 11(a)] differs significantly from the patterns presented in Figs. 10 and 11. The hot spots in the yellow beam indicate a self-focusing process. It should be noted that the values of λ_Y correspond to the center of gravity of the spectral distribution of the conical emission. The conical emission itself is a broadband one, as illustrated on Fig. 2. The short-wavelength wing of this emission expands over more than 0.4 nm, which indicates that a nonnegligible part of the spectral content of the emission propagates under self-focusing conditions. Because of the reduced integral intensity of these components, self-focusing itself is difficult to obtain, but we attributed the characteristic distribution to a modulational instability of this part of the emission at $n_2^{SPM}(\lambda_Y') > 0$. The remaining part of the frequency content of the emission evolves in space to an even broader ring of a decreas-

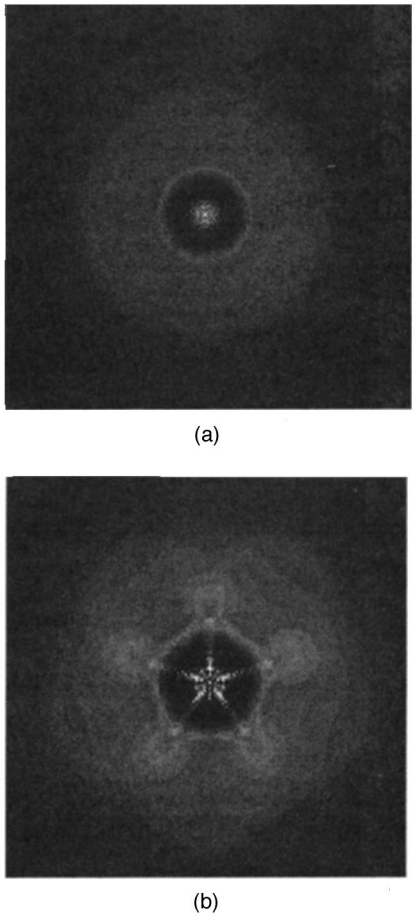

(a)

(b)

Fig. 11. Simulation results for $\lambda_L = 329.825$ nm ($\lambda_Y = 590.0$ nm): (a) nonlinear medium without fluctuations (the beam is focused in the center); (b) nonlinear heterogeneous medium (the symmetry in the picture is due to the symmetry in the perturbation).

ing radius [the background of the hot spots in Fig. 11(a)]. Possible sources of perturbations inside the nonlinear medium are the inhomogeneities in the Na vapor density. Sometimes the hot spots reproduced their spatial positions, which could be explained by the perturbations introduced by the diffraction from the iris-diaphragm knifes. Fig. 11(b) presents a gray-scale image of the simulation of the yellow emission evolution under conditions, identical to those for Fig. 10(b), but at $n_2^{\mathrm{SPM}} > 0$. The symmetrical pattern formed is a result of the symmetrical perturbation of the initial ring profiles [see Eq. (9)]. Initial modulation depth was chosen to be 0.1.

4. CONCLUSION

In this work we presented experimental data and numerical simulations of yellow conical emission observed in sodium vapor excited by laser pulses tuned near to the 3^2S-4^2P resonant transitions. An explanation of the nonmonotonical tuning of conical emission is suggested by the conditions, under which the accompanying resonant-enhanced nonlinear processes of SPM and IPM do not disturb the linear (versus intensity) vector synchronism of the FWPM. The characteristic spatial evolution of the conical-emission pattern at relatively large and decreasing detunings of the pump versus the $3S-4P$ resonance could be attributed, at least in part, to the 2D spatial SPM of the broadband yellow conical emission under highly dispersive nonlinearity in the vicinity of the D_2 line of Na.

From the good qualitative agreement between the experimental and simulation results we conclude that the nonlinear processes SPM and IPM, accompanying the FWPM observed, strongly influence the spectral and spatial features of generated conical emission.

Further and more detailed analysis of the processes should account simultaneously for the FWPM and spatial evolution of all the waves involved.

ACKNOWLEDGMENTS

The authors thank the head of the Institute for Experimental Physics, H. Jäger, for continuous support. S. Dinev, A. Dreischuh, and V. Kamenov are grateful to the Technical University Graz, Institute for Experimental Physics, for the warm hospitality during their research stays. A. Dreischuh was a fellow of Österreichischer Akademischer Austauschdienst. V. Kamenov was a fellow of the Central European Exchange Program for University Studies Program (Network A-21). This work was supported partially by the Austrian Science Foundation (project P9929) and the National Science Foundation, Bulgaria.

*Permanent address: Department of Physics, Sofia University, 5 J. Bourchier Boulevard, BG-1164 Sofia, Bulgaria.

REFERENCES

1. Y. M. Kirin, S. G. Rautian, A. E. Semenov, and B. M. Chernobrod, JETP Lett. **11**, 226 (1970).
2. D. J. Harter and R. W. Boyd, Phys. Rev. A **29**, 739 (1981).
3. R. W. Boyd, M. G. Raymer, P. Naurum, and D. J. Harter, Phys. Rev. A **24**, 441 (1981).
4. W. Chalupczak, W. Gawlik, and J. Zachorowski, Opt. Commun. **99**, 49 (1993).
5. Y. Shevy and M. Rosenbluh, J. Opt. Soc. Am. B **5**, 116 (1988).
6. U. Domiaty, D. Gruber, L. Windholz, S. G. Dinev, M. Allegrini, G. de Fillipo, F. Fuso, and R. H. Rinkleff, Appl. Phys. B **59**, 525 (1994).
7. A. C. Tam, Phys. Rev. A **19**, 1971 (1979).
8. E. A. Chauchard and Y. H. Meyer, Opt. Commun. **52**, 141 (1984).
9. M. E. Cernshaw and C. D. Cantrell, Phys. Rev. A **39**, 126 (1989).
10. N. V. Lugovoi and A. M. Prokhorov, Sov. Phys. JETP **42**, 42 (1975).
11. I. Golub, R. Shuker, and G. Erez, Opt. Commun. **57**, 143 (1986).
12. L. You, J. Mostowski, J. Cooper, and R. Shuker, Phys. Rev. A **46**, 2925 (1992).
13. L. You, J. Mostowski, J. Cooper, and R. Shuker, Phys. Rev. A **46**, 2903 (1992).
14. M. LeBerre, E. Ressayre, A. Tallet, K. Tai, H. M. Gibbs, M. C. Rushford, and N. Peyghambarian, J. Opt. Soc. Am. **1**, 591 (1984).
15. J. F. Valley, G. Khitrova, H. M. Gibbs, J. W. Grantham, and J. Xu, Phys. Rev. Lett. **64**, 2362 (1990).
16. Y. Silverberg, Opt. Lett. **15**, 1282 (1990).
17. A. Dreischuh, U. Reiter-Domiaty, D. Gruber, L. Windholz, and S. Dinev, Appl. Phys. B (to be published).
18. P. Sorokin and J. Wynne, in *Nonlinear Infrared Generation*, Y. R. Shen, ed., Vol. 16 of Topics of Applied Physics (Springer, Berlin, 1977), p. 160.
19. J. F. Raintjes, ed., *Nonlinear Optical Parametric Processes in Gases and Liquids* (Academic, Boston, Mass., 1988).
20. R. Alfano and P. Ho, "Self-, cross-, and induced-phase modulation of ultrashort laser pulse propagation," IEEE J. Quantum Electron. **QE-24**, 351 (1988).
21. R. B. Miles and S. E. Harris, "Optical third-harmonic generation in alkali metal vapors," IEEE J. Quantum Electron. **QE-9**, 470 (1973).
22. S. Dinev and A. Dreischuh, "Sum-frequency generation in the xuv," Opt. Quantum Electron. **23**, 91 (1991).
23. Y. Prior, "A complete expression for the third-order susceptibility: perturbative and diagrammatical approach," IEEE J. Quantum Electron. **QE-20**, 37 (1984).
24. R. Saxena, I. McMichael, and P. Yeh, "Dynamics of refractive-index changes and two-beam coupling in resonant media," Appl. Phys. B **51**, 243 (1990).
25. G. Yang and Y. R. Chen, "Spectral broadening of ultrashort pulses in a nonlinear medium," Opt. Lett. **9**, 510 (1984).
26. R. H. Lehmberg, J. Reintjes, and R. C. Eckardt, "Two-photon resonantly enhanced self-defocusing in Cs vapor at 1.06 mm," Appl. Phys. Lett. **25**, 374 (1974).